Interpretative Generative Deep Learning Hurdle Models Unraveled Functional Diversity Shifts in Bird Communities with Sea Level Rise

Liying Li[1], Junwen Bai[2], Shoukun Sun[3], Marcos Zuzuaggrei[4], Daniel Fink[2], Zhe Wang[1], Heather Lahr[1], Courtney Scarborough[1], Caitlin Young[5]

1.National Center for Ecological Analysis and Synthesis, Santa Barbara, California, United States 2. Cornell University, Ithaca, New York, United States 3. University of Idaho, Idaho Falls, Idaho, United States 4. School of Engineering, University of California, Merced, Merced, California, United States 5. National Oceanic and Atmospheric Administration

Abstract

Coastal bird communities on the northern Gulf Coast are being reshaped by sea-level rise (SLR) and land-use change. Most forecasts on biodiversity change stop at occurrence or richness and rarely integrate the consequences of functional diversity change across scales. Interactions between SLR and reserve-scale nutrient/productivity changes, and their impacts on species, are understudied and seldom quantified for decision-making use. This study mapped abundance for 350 species under historical vs. SLR scenarios using generative deep hurdle models. These models decomposed drivers into abiotic environmental envelopes and species–species associations. Three functional trait spaces (foraging, movement, and social behavior) change was analyzed via trait probability density analysis at regional and reserve scales (with simulated primary productivity change under SLR). SLR yields species redistribution rather than uniform collapse. A small set of abiotic gradients (elevation/inundation, marsh extent, shoreline proximity) dominates abundance patterns, while biotic structure refines local composition. Trait analyses reveal scale-dependent patterns: region-wide, the occupied trait space shrinks or redistributes, characterized by higher evenness and lower richness and redundancy. In reserves, productivity effects broaden foraging trait space, compress movement trait space toward intermediates, and narrow but differentiate social behavioral space (lower redundancy, stronger extremes). Climate-adapt conservation should secure landward migration corridors and prioritize parcels adjacent to tidal channels and inlets where models predict persistent suitability, and tune reserve-scale productivity management to preserve functional diversity. By linking spatial redistribution, community structure, and trait dynamics—and by summarizing the limitations of habitat-specific models—this work addresses critical gaps and provides actionable indicators for coastal conservation planning in the face of environmental changes.

Introduction

There are mounting threats to biological diversity from global environmental change and human activities (Olden et al., 2008). Birds exemplify the consequences of these threats: habitat loss and degradation, fisheries bycatch (for seabirds), pollution, prey depletion, and climate variability have driven widespread population declines and eroded functional diversity in birds (Dias et al., 2019; Rosenberg et al., 2019; Saintilan et al., 2014). Superimposed on these drivers, sea-level rise (SLR) is rapidly altering coastal geomorphology and flooding regimes, with the IPCC and U.S. federal assessments projecting substantial increases in chronic high-tide flooding and storm-driven extremes on multi-decadal horizons, thereby compressing ("squeezing") intertidal habitats critical to coastal birds (NOAA, 2022). Tidal-marsh specialists experience more frequent spring-tide nest inundation and lowered productivity—well documented for Saltmarsh Sparrow, where flooding is common even today and expected to worsen with accelerating SLR

(Bayard & Elphick, 2011; Cook et al., 2024). Beach-nesting shorebirds (e.g., Piping Plover) face direct loss and fragmentation of supratidal nesting habitat and higher probabilities of storm-surge overwash; projections at barrier-island systems show substantial declines in suitable breeding area under SLR scenarios, even as post-storm sediment dynamics can occasionally create transient habitat patches (Seavey et al., 2011). Migratory shorebirds also risk diminished carrying capacity at stopover sites as intertidal foraging flats drown or are pinched against hardened shorelines, reducing roosting options and energetic refueling opportunities(Galbraith et al., 2005). For seabirds on low-lying oceanic islands, SLR combined with storm waves and groundwater rise elevates overwash risk, nest failure, and colony displacement, highlighting the need for higher-elevation refugia and assisted colonization in some archipelagos (Reynolds et al., 2015). Together, these processes indicate that avian population declines increasingly translate into functional erosion via the selective loss of flood-sensitive foraging and breeding strategies—underscoring the need for trait-explicit analyses embedded in standardized frameworks to forecast ecosystem consequences and guide adaptation (Intergovernmental Panel on Climate Change (IPCC), 2023).

Species distribution models (SDMs) provide a practical framework for interpolating species' distributions across space and time from occurrence and/or abundance records (Botella et al., 2018), enabling the estimation of biodiversity metrics and scenario-based forecasting of environmental or anthropogenic change (Elith & Leathwick, 2009; Pearson & Dawson, 2003). Recent advances in machine learning and deep learning have improved predictive performance by capturing non-linear responses and spatial structure and by integrating heterogeneous data sources (e.g., remote sensing, environmental covariates, citizen-science observations) (Adadi, 2021). Artificial intelligence-driven species distribution models have attracted attention for their practical utility for conservation planning, risk assessment, and ecological forecasting. For example, Lee et al. (2022) predicted the spread of invasive species under climate change, Ennakri et al. (2025) presented how AI SDMs support biodiversity monitoring at scale, and Ryo et al. (2020) informed conservation decision-making through interpretable and ecologically grounded models.

The superior predictive accuracy of artificial intelligence to capture complex, non-linear relationships and spatial patterns leads to improved accuracy, especially for less-represented species (Botella et al., 2018). They can also leverage spatial environmental tensors and remote sensing imagery to extract ecological features and spatial patterns not captured by traditional models. Transfer learning and foundation-model approaches further extend SDMs to data-sparse species via few-shot and zero-shot inference (Dinnage, 2024). Generative and masked-autoencoder strategies have yielded high discrimination and calibration across diverse taxa and large occurrence datasets (Yan et al., 2024). In addition, most traditional SDMs require the specified species records format, namely presence-only, presence/absence, or pseudo-presence/absence (Phillips, 2008). Deep learning also doesn't discard spatial and temporal autocorrelation—key signals for distributional patterns (Botella et al., 2018), while traditional machine learning does.

Despite these advances, significant gaps remain. Most research progress has been made in quantifying species abundance and richness, which are used as correlates of functional diversity. Functional traits are morphological, physiological, or behavioral features of organisms that can be quantified at different organizational levels, from individuals to ecosystems. With changes in habitat, species with poorly adapted traits are likely to disappear. In communities with functional redundancy, the loss of one species can be buffered by others occupying similar trait space, whereas in communities where redundancy is low—or where functionally unique species are lost—ecosystem functioning can decline disproportionately (Biggs et al., 2020; Violle et al., 2017).

Single-species distribution models that focus on taxonomic units (species/genus) are poorly suited to forecast how environmental change reshapes communities and their ecosystem functions (MCGILL et al., 2006). (MCGILL et al., 2006). A trait-based perspective to community ecology can discover how ecosystem functions of communities vary along environmental gradients (Violle et al., 2007) (historical and sea level rise scenarios in this study).

Moreover, most pipelines still decouple species–environment relationships from species–species dependence, even though both operate jointly in nature. Most importantly, modeling species abundance is rarely explored in deep learning, which restricts our understanding of demographic changes in species in response to environmental and anthropogenic changes (Thuiller et al., 2004). Addressing these gaps requires a closed-loop framework that synthesizes environmental drivers and interspecific associations, as well as the abundance and functional diversity of species and communities, within a unified architecture.

This study introduces a generative deep learning hurdle framework with trait probability density analysis that addresses these gaps. We (i) integrate environmental drivers with species trait embeddings to connect traits → niches → functions; (ii) model residual species–species dependence alongside spatial–temporal structure to reflect co-occurrence beyond shared environment; and (iii) adopt a hurdle likelihood to handle zero inflation by modeling occurrence (Bernoulli–logit) and positive abundance conditional on presence (e.g., Poisson or Negative Binomial) separately (Edmondson et al., 2021). Applied to birds of different habitats, our approach yields spatially explicit forecasts of presence probability, conditional and marginal abundance, and derived functional diversity under present conditions and SLR scenarios—providing decision-relevant guidance for conservation and adaptation.

Method

Study area and data

Analyses were conducted at 3km*3km spatial resolution on the northern Gulf of Mexico coast, including the southeastern parishes of Louisiana, the coastal counties of Mississippi and Alabama, and the western counties of the Florida panhandle. The study area aligned with the National Centers for Coastal Ocean Science project on Predicting Impacts of Sea Level Rise in the Northern Gulf of Mexico (NCOOS, 2017). All the required simulated data to create a sea level rise scenario are available for this study area, such as Bathymetry DEM (NOAA National Geophysical Data Center, 2010) and marsh productivity change with sea level rise for three National Estuarine Environmental Research Reserves: Apalachicola, FL, Weeks Bay, AL, and Grand Bay(Alizad et al., 2016). This research draws on findings from studies examining the impact of sea level rise on coasts and coastal habitats, translating them into species response information to inform conservation and ecosystem management.

We used observation records from eBird (Sullivan et al., 2009) from 2019 to 2021, which included up to 115,575 checklist occurrences and counts, along with sampling-event metadata (e.g., protocol, duration, distance traveled, number of observers, start time). Data was acquired and merged into one year for data augmentation. Checklists of all species were summarized into a table of species observations, with each shared locality ID represented as a single row in the table. The data version used in this study was the eBird Reference Dataset from 2025. To derive detections and non-detections, we restricted analyses to Complete Checklists—checklists where observers report all species they could identify during the sampling event—so that species not reported can be treated as absences on that checklist. Species responses were aggregated to the

modeling grid with a 1km buffer. We modeled all 350 bird species within the study area for two targets per 3km*3kmgrid cell: (i) occurrence (presence/absence) and (ii) abundance/count (non-negative), only excluding species with fewer than 10 observations over the three years through January, 2019 to December, 2021. Taxonomy and nomenclature follow the eBird taxonomy 2020.

Environmental covariates were assembled, tabulated, and standardized prior to modeling. Predictors included: topography (Amatulli et al., 2018)—mean elevation, elevation variability, slope, and aspect decomposed to northness and eastness; Land cover—proportional cover from C-CAP/land-cover classes aggregated to the grid (NOAA, 2024); climate-mean temperature and temperature range, and primary productivity of ecosystem- biomass concentration, and chlorophyll concentration. A full description of the list of data used and data sources can be found in this Supplementary Information. A climate change and sea level rise scenario is created by modifying the historical prediction surface with replaced temperature under climate change from Bio-ORACLE (Assis et al., 2024) and WorldClim2 (Fick & Jijmans, 2017) for ocean and land, respectively, and land cover classes with marsh migration (Marcy et al., 2011) (accessed at https://coast.noaa.gov/slrdata/). The projected temperature was acquired for CMIP6 SSP5-8.5, matching the intermediate high sea level rise scenario (1.2 m above the mean sea surface level by 2100) (Parris et al., 2012). We utilized Mean High Water and Salt Marsh Productivity data from the NOAA National Centers for Environmental Information (Alizad et al., 2018), which were modeled using Hydro-MEM (Alizad et al., 2016), to modify the historical bathymetry, digital elevation, and primary productive predictors (biomass concentration and chlorophyll concentration)for the three National Estuarine Research Reserves.

To enable trait-based comparisons, species were cross-walked to a curated trait table via eBird taxonomy and the AVONET bird species trait table (Tobias et al., 2022a). Categorical traits, including Habitat, Primary Lifestyle, Trophic Level, Trophic Niche, and Migration status, were used to categorize trait probability density, trait analysis, and draw separate graphs. Continuous traits, such as Tarsus Length, Habitat Density, Tail length, and wing length, were used for trait probability density (TPD) surface estimation, with non-zero support delineated for interpretability.

Generative Variational Autoencoder with Gaussian Mixture

Utilizing citizen science data for species occurrence and count observations requires a robust model structure to account for data noise across time and space (Elith et al., 2006). AI SDMs have been proven to outperform traditional machine learning models to handle such noise (Lee et al., 2022). We follow a generative framework of Gaussian Mixture Variational Autoencoders (Bai et al., 2021a), which allows for zero-shot learning (predicting for species not seen during training) (Yan et al., 2024). The architecture consists of two parallel encoders, feature and label encoders, a shared latent representation, and two decoders, each designed to align and reconstruct feature and label modalities (Figure 1).
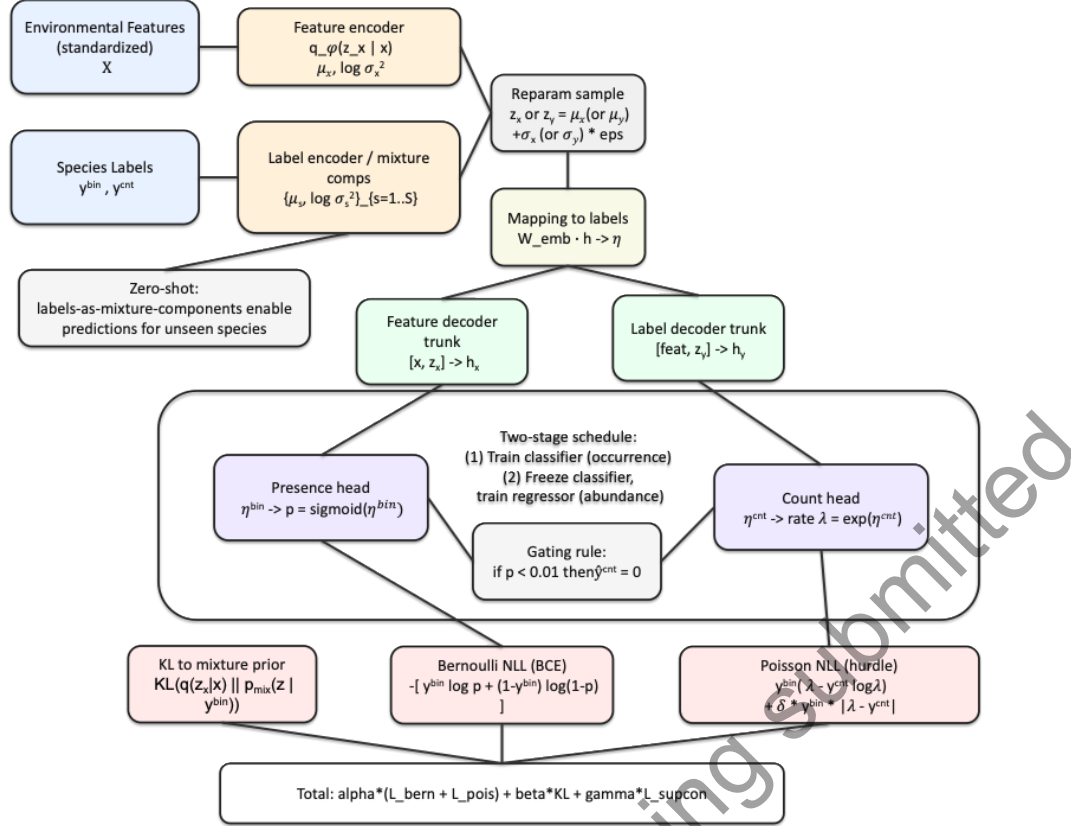
Figure 1. Diagram of the Generative Variational Autoencoder with Gaussian Mixture in a hurdle framework (gate rule, conditional Poisson loss, and two-stage training schedules) for species abundance predictions

Environmental feature vectors X at a location/time (e.g., land-cover fractions, elevation stats, temperature means/ranges, chlorophyll, etc.) were first standardized and then passed through three fully connected layers (256, 512, 256 units) with rectified linear unit (ReLU) activations and dropout regularization. Outputs μ_x (mean), $\log \sigma_x^2$ (log variance) are mapped to a latent Gaussian distribution, and reparametrized by μ_x and $\log\sigma_x^2$), generating a reparametrized latent sample Z_x for the feature label path. Species occurrence or abundance labels j were embedded and projected through a symmetric encoder consisting of fully connected layers (embedding dimension $\rightarrow$ 512 $\rightarrow$ 256 units) with ReLU activations and dropout. The resulting output (mean μ_s, variance $\log \sigma_s^2$ per species) was parameterized into a Gaussian distribution. Reparameterization trick that ensured differentiability while capturing uncertainty in the latent variables:

$$z=\mu+\epsilon\odot\sigma, \epsilon\sim N(0,I).$$

And each label was further modeled as a component of a Gaussian mixture, enabling mixture-based latent modeling. The Gaussian Mixture Variational Autoencoder (GMVAE) prior (J. Bai et al., 2021a) in the latent space allows each species label to be associated with a distinct mixture component, supporting zero-shot prediction (Yan et al., 2024).

Both encoders produced distributions from which latent codes were sampled using the Latent variables were passed through two decoding pathways: The Feature Decoder h_y concatenated latent codes with input features and projected them through two fully connected layers to generate normalized embeddings in the shared space. The Label Decoder h_x concatenated latent codes with feature embeddings and projected them through fully connected layers with leaky ReLU activation to generate label embeddings. A reconstruction branch directly attempted to

reconstruct the original features from the latent codes, ensuring information preservation. Both feature and label decoders were aligned into a shared embedding space. A learned linear transformation then mapped embeddings back into the label space ($W\_emb \cdot h \rightarrow \eta$), enabling final predictions of species occurrence probability or abundance.

Model training was conducted using Pytorch Lightning (Falcon, 2019) with GPU acceleration where available. The Adam optimizer was applied with a separate initial learning rate of $5e^{-3}$ and $2e^{-4}$ for classification and regression, respectively, decayed by a factor of 0.5 if validation loss did not improve for four epochs using a StepLR scheduler. All experiments were repeated across 70%/15%/15% train/validation/test partitions using a fixed random seed (42) to ensure robustness, and results were reported as the mean ± standard deviation of evaluation metrics. TorchMetrics was used for accuracy, RMSE evaluation. Models were trained for a maximum of 500 epochs each for classification and regression. The regressor VAE was trained while the classifier was frozen/evaluation. During this phase, the regressor consumed the classifier's sigmoid presence probabilities (computed without gradient) to gate abundance predictions. No gradient clipping and no early stopping were applied. The mini-batch size was 4096 for all experiments.

Each VAE uses the same internal components as described above (feature encoder/decoder and label encoder/decoder) but is trained with task-specific likelihoods inside a composite objective. Let L_{NLL} denote the prediction negative log-likelihood terms (both the label-decoder path and two feature-decoder-based–based paths), L_{KL} the latent KL divergence (GMVAE regularization) (Kingma & Welling, 2022), and L_{CPC} the contrastive alignment loss (Bai et al., 2021b; Khosla et al., 2021). Loss contributions were weighted such that NLL received primary emphasis (α=10), KL divergence was scaled by β=6 to balance reconstruction and regularization, and CPC alignment was scaled by γ=1 (Kong et al., 2020). During training, the weighted sum of loss was minimized:

$$\mathcal{L}_{total} = \alpha \cdot (\mathcal{L}_{NLL,Label} + \mathcal{L}_{NLL,feat} + \mathcal{L}_{NLL,feat2)} + \beta \cdot \mathcal{L}_{kl} + \gamma \cdot \mathcal{L}_{CPC}$$

Two-stage hurdle structure

A two-stage hurdle approach (Kong et al., 2020) was used to model species abundance distribution for 350 species. A hurdle model is a two-part model that specifies two separate processes, one for generating zero values and another for generating values given that they are non-zero, for handling count observations with excess zeros (Edmondson et al., 2021)

In this study, the first stage is using the Multivariate Probit Model (Chen et al., 2016) to model the presence/absence of each species, capturing interspecies and environment–species covariance. (Bai et al., 2020). This stage is treated as a *foundation model* (Dinnage, 2024), that provides ecological context. Building on the occurrence distribution, a second fine-tuned regression abundance model was trained using species count data with rich context informed by the occurrence model. For classification, the label decoder projects into a probability space through a sigmoid output layer, yielding predicted occurrence probabilities for each species (Presence head: ηbin $\rightarrow$ p = sigmoid($\eta^{\wedge}bin$)). For regression, the decoder projects into a continuous output layer with linear activation, providing predicted species abundances.

Because both tasks share the same latent embedding, gradients from classification and regression jointly shape the latent space (Count head: ηcnt $\rightarrow$ rate λ = exp(ηcnt)). This encourages the model to learn representations that are predictive of both species presence/absence and relative

abundance, rather than optimizing them in isolation; therefore, it was named as cross-task regulation. This integration allows the model to flexibly shift between predicting occurrence and abundance depending on available data, while maintaining a unified ecological embedding space.

The NLL loss uses a hurdle formulation with two probabilistic heads: a Bernoulli component for presence and a Poisson component for conditional counts (Bishop, 2016; Huffer et al., 2008). During the occurrence (classification) phase, the classifier outputs a logit $\eta_{is}^{(bin)}$, converted to a probability $p_{is}=\sigma(\eta_{is}^{(bin)})$ with the logistic sigmoid $\sigma(\cdot)$. The Bernoulli negative log-likelihood (equivalently, binary cross-entropy), averaged over samples and species, is

$$\mathcal{L}_{bern} = -\frac{1}{NS}\sum_{1=1}^{N}\sum_{s=1}^{S}[y_{is}^{bin}logp_{is} + (1 + y_{is}^{bin})\log(1 - p_{is})]$$

Let x_i denote environmental features for sample $i=1,...,N$ and $y_{is}^{bin}\in\{0,1\}$ the presence/absence of species $s=1,...,S$. When present, the observed count is $y_{is}^{cnt}\in N$.

During the Abundance (regression) phase, the standard GLM Poisson log-likelihood with log link (Cameron & Trivedi, 2013; Kingma & Welling, 2022) was used, which was restricted to the positive (post-hurdle). The regressor outputs an unconstrained value $\eta_{is}^{(cnt)}$ that parameterizes the Poisson rate $\lambda_{is}=exp(\eta_{is}^{(cnt)})$. A small L_{aux} auxiliary term to stabilize rate estimates. Counts are modeled only when a species is present via the hurdle mask $m_{is}=y_{is}^{bin}$. The presence indication masked the Poisson loss to respect the hurdle structure.

$$\mathcal{L}_{pois} = \frac{1}{\sum_{i,s}m_{is}}\sum_{i=1}^{N}\sum_{s=1}^{S}m_{is}(\lambda_{is} - y_{is}^{cnt}log\lambda_{is})$$
$$\mathcal{L}_{aux} = \delta\frac{1}{\sum_{i,s}m_{is}}\sum_{i,s}m_{is}(\lambda_{is} - y_{is}^{cnt})$$

For evaluation of occurrence during training/validation/test, raw sigmoid scores (probability) from the classifier's feature path are converted to binary with data-adaptive thresholds computed per species from the batch's column mean (probability > mean is 1 otherwise 0 for high-to-mid prevalence species (probability mean > 0.01), Probability > fixed threshold 0.05 is 1 otherwise 0 for Low-prevalence species).

During regressor training, the classifier's probabilities are used to gate abundance predictions: if presence probability < 0.01, predicted abundance is set to 0. Bias is more prominent in count observations. Observers may record thousands of birds without counting them; therefore, the larger the count is, the bigger the error may be. To mitigate observer-related biases, we train the abundance model using log-transformed counts rather than raw counts. Predictions are then back-transformed to the original scale and rounded to integers for evaluation with mean squared error (MSE).The alignment between where species are present and the predicted number of individuals is assured by the Contrastive Learning (Bai et al., 2021c). Occurrence and abundance predictions are linked through the shared latent space: the presence model constrains abundance estimates, encouraging the hybrid model to learn biologically realistic joint representations of occurrence and abundance.

Classification and regression were evaluated using different sets of metrics. Classification used Accuracy, F1-score, Precision, Recall, and Intersection over Union (IoU). These metrics captured different aspects of predictive performance, with IoU providing a robust measure of overlap between predicted and observed species presence. Additionally, reliability diagrams and Brier scores were used to assess the degree to which predicted probability models matched observed frequencies. Regression used Root Mean Squared Error (RMSE) and Mean Absolute Error (MAE). RMSE emphasized large deviations between predicted and observed abundance

values, while MAE provided a more interpretable measure of average prediction error. Together, these metrics provided a comprehensive evaluation of predictive accuracy, robustness, and ecological interpretability across the two modeling tasks.

For downstream analyses, we saved monthly prediction surfaces and summary arrays for evaluation metrics (e.g., F1, precision/recall, calibration, richness, and community dissimilarity indices). The trained model also yields a 512-dimensional feature embedding per species (array shape 350×512) and a 350×350 residual correlation embedding used to interrogate interspecific co-occurrence patterns beyond environmental effects.

Trait Density Probability Analysis

Species traits were sourced from AVONET (Tobias et al., 2022b), a global compilation of avian morphology and ecology with species-level summaries derived from >90,000 measured individuals across 11,000+ species. However, only species-level mean traits were provided in AVONET. Intraspecific trait variation arising from genetic differences and phenotypic plasticity can be large enough to alter interaction outcomes and community assembly. Therefore, consideration of stochasticity in intraspecific trait differences is required to reduce the risks of biasing trait distribution change predictions with environmental changes. Therefore, we used continuous trait summaries in AVONET as standardized means for species-level continuous traits and categorical traits as categorical assignments.

Continuous traits were converted to pseudo-individual values by parametric jittering with independent Gaussian draws using the species-level means from AVONET. A conservative coefficient of variation (5%) was imposed to reflect unobserved within-species variability in the absence of trait-specific variance estimates from AVONET. To align traits with our observation table, we expanded each species' trait record to the number of observations for that species (n_s). When the trait was missing or zero, values were left as NA. Categorical traits (e.g., trophic niche, habitat, migratory status) were replicated deterministically across the n_s rows. This strategy preserves species identity while yielding an observation-aligned trait matrix in which continuous traits incorporate modest within-species dispersion to accommodate intraspecific variation that affects community assembly (Bolnick et al., 2011) when only species means are available.

We quantified species' functional structure using the Trait Probability Density (TPD) approach implemented in the R package TPD. The TPD framework represents each ecological unit (species, community) by a probability density function in trait space, enabling overlap-based measures of richness, dissimilarity, redundancy, and divergence.

Continuous traits (and, where mixed traits were present, ordination scores from) were scaled to zero mean and unit variance before analysis. Species-level probability densities were estimated using multivariate kernel density estimation, and returns species/population TPDs were evaluated on a regular grid. We set the probability isopleth at alpha = 0.95 to define the high-probability support (non-zero region) and controlled grid resolution via two divisions. We didn't use a Gower–PCoA reduction to analyze the mixed traits space of continuous traits and categorical traits. Instead, we categorize species by their categorical traits and built three pair-wise 2-dimensional trait spaces, namely Beak Length/Beak Depth (indicating foraging trait space), Tail length/Hand Wing Index (indicating movement trait space), and Tarsus Length/Habitat Density (Indicating social behavior space). Tarsus length represents species size, and we regard species of different size as have distict social behavior

From species to communities, community-level densities were obtained for each of the three spaces, which mixes species probability density, weighted by their relative abundances in each sampling unit (here we used historical and sea level scenarios). This produces the Trait Probability Density (TPD) for each scenario, which is directly comparable for evaluating species resilience in response to sea level rise. We summarized and reported the functional structure using richness, evenness, redundancy, and divergence, all of which were computed on the probabilistic trait space. All analyses were conducted in R programming language (R core team, 2021)

Results

Population abundance shifts upward in the estuary

The generative deep hurdle model produced abundance maps for bird species, comparing the historical baseline to the sea-level-rise (SLR) climate scenario in the northern Gulf Coast (Figure 2). Abundance values are expected abundance derived by multiplying predicted occurrence probability by predicted counts. Each panel uses a different color (value) range (e.g., the egret/heron scales top out around ~10–12.5, while the crow reaches into the thousands). Across species, coherent coastal bands in the historical maps break into patchier inland clusters under SLR, especially along major waterways—indicating displacement rather than uniform decline. The scenario maps showed persistence clustering along tidal creek networks and near estuary mouths, while back-barrier/impounded cells lose suitability—i.e., places with better tidal exchange fare better. The hotspot of species distribution geography becomes more fragmented as a result of adaptation to sea level rise. The highest losses occur where inland migration is blocked by roads/levees, while sites connected to channels retain or gain suitability.

Zooming to wetland specialists, a contract near the coast and a shift up-estuary were observed. For example, high-abundance cells of Great Egret and Great Blue Heron, located along the immediate shoreline, weaken under SLR, with hotspots reappearing along river mouths and in higher-elevation marsh and back-bay zones inland. This pattern is consistent with tidal-marsh "coastal squeeze," where inundated lowlands are not fully replaced inland. Forest birds, such as the Carolina Wren and Red-bellied Woodpecker, show a modest coastal retreat but retain strong interior holdouts. They observed a reduction in abundance in low-lying coastal forests under SLR, while interior upland/river-corridor cells remained stable or intensified. The signal suggests their sensitivity to flood-driven habitat change at the coastal fringe, but resilience persists where canopy structure remains intact inland. American Crow and House Sparrow are generalists displaying the smallest scenario deltas. Abundance remains comparatively stable, with slight inland shifts tracking developed corridors and higher ground. A diffuse interior presence with subtle redistribution offsets any local coastal dips of species abundance. In sum, local coastal losses redistribute abundance inland and up-estuary for wetland birds, cause minor edge retreats for forest birds, and leave generalists essentially unchanged aside from subtle inland shifts. The losses at the lowest elevations are compensated by persistence inland abundance, which is consistent with landward habitat migration constrained by topography and development.
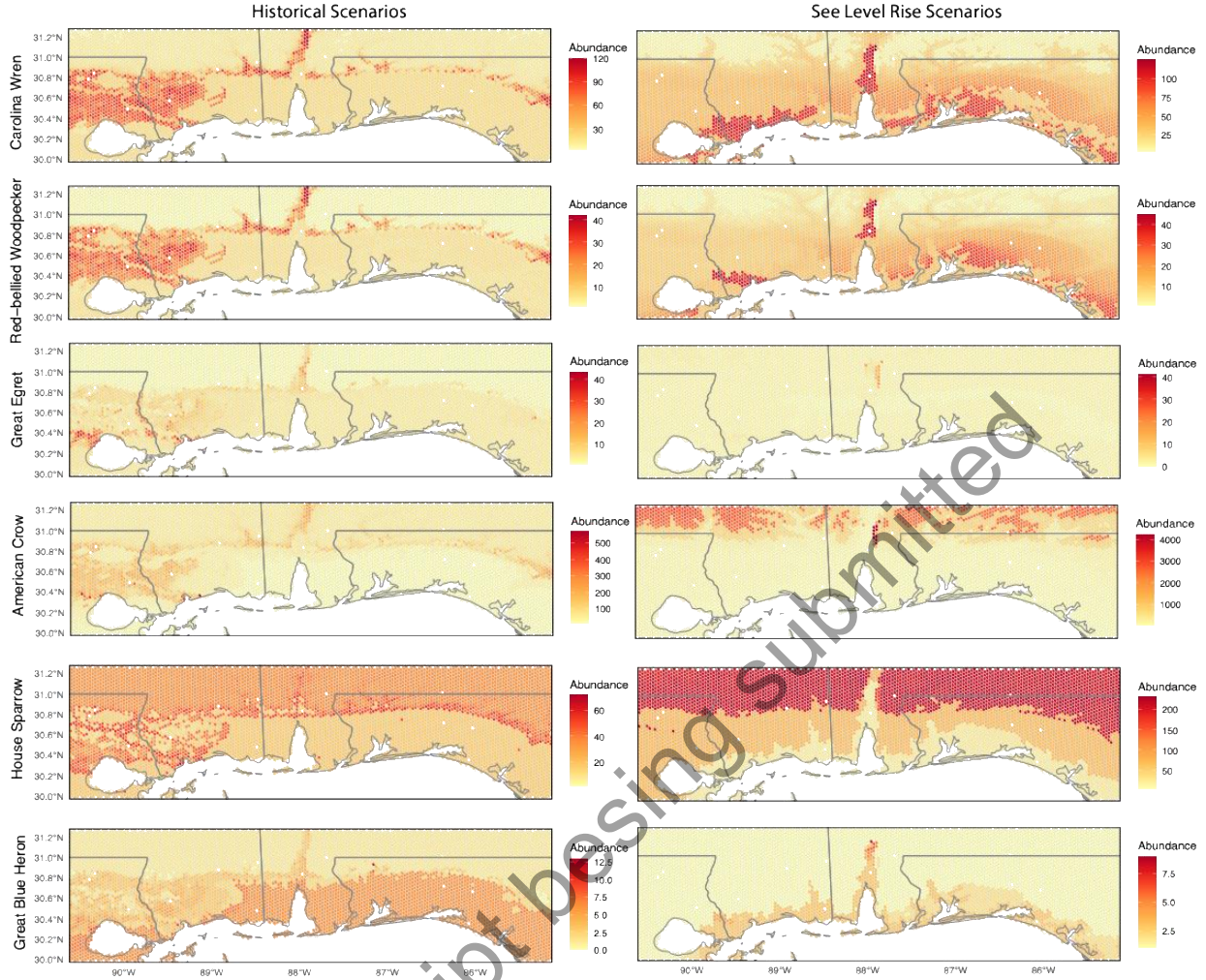
Figure 2. Species abundance distribution shifts from historical scenarios and sea level rise scenarios

Interspecific relations and environmental envelope

We assembled a paired dataset combining environmental grids used for predictions and the predicted abundance expectation from the Deep Hurdle model. A monotonic association using Spearman's rank correlation was calculated for each species abundance expectation and feature at the same prediction grid. Spearman ρ is robust to nonlinearity and scale differences common in ecological predictors and count-like responses. Operationally, each column of Y was rank-transformed over each aligned environmental predictor row, standardized (zero mean, unit variance), and computed as a Pearson correlation on the ranks. Collecting all pairs yields a species × feature association matrix $\mathcal{R}_{sf}$. An agglomerative hierarchical clustering (average linkage) was applied to the dissimilarity (1- $\mathcal{R}$), with γ clipping to [-1,1] for stability. And rows and columns were reordered according to the order of the dendrogram's leaves.

Positive Spearman ρ indicates that species' expected abundance tends to increase with the correlated feature across the sampled gradient; negative values indicate the opposite tendency. Blocks of warm/cool colors after ordering highlight guilds of species sharing similar environmental associations and feature sets that covary in their effects across species (Figure 3).

The rank-ordered correlations show a steep drop-off after the top few variables, indicating that a small set of environmental gradients dominates the focal species' spatial pattern. The long tail of low-magnitude bars suggests secondary gradients have limited or context-dependent effects on species abundance. In practical terms, the species' distribution is primarily filtered by a handful of abiotic constraints; management actions should prioritize those that modify these environmental constraints, such as particular habitat availability and elevation buffers, which the species chooses, as these are most likely to shift species abundance.

We summarized species–species associations in the model's label embedding space by computing a pairwise correlation matrix among species' embedding vectors. We first mean-centered each vector across embedding dimensions. Then we calculated Pearson correlations, yielding a species-by-species symmetric matrix $\mathcal{R}_{ss}$ with a unit diagonal (Set the diagonal to 0 for visualization only). Again, an agglomerative hierarchical clustering (average linkage) was applied to the dissimilarity (1 - R), with γ clipping to the range of [-1, 1] for numerical stability (Figure 3).

For visualization, we set the diagonal to zero (display only). Hence, the color scale emphasizes interspecific associations, and we scaled the colormap limits to the 2nd–98th percentiles of off-diagonal values to enhance contrast while remaining robust to outliers.

The resulting ordered correlation heat map provides a compact view of species that share similar or dissimilar embedding profiles—i.e., species predicted to exhibit positive residual association indicate similar abiotic niche (warm colors) or contrast indicate dissimilar abiotic niche (cool colors), based on the learned label embedding space from observations.
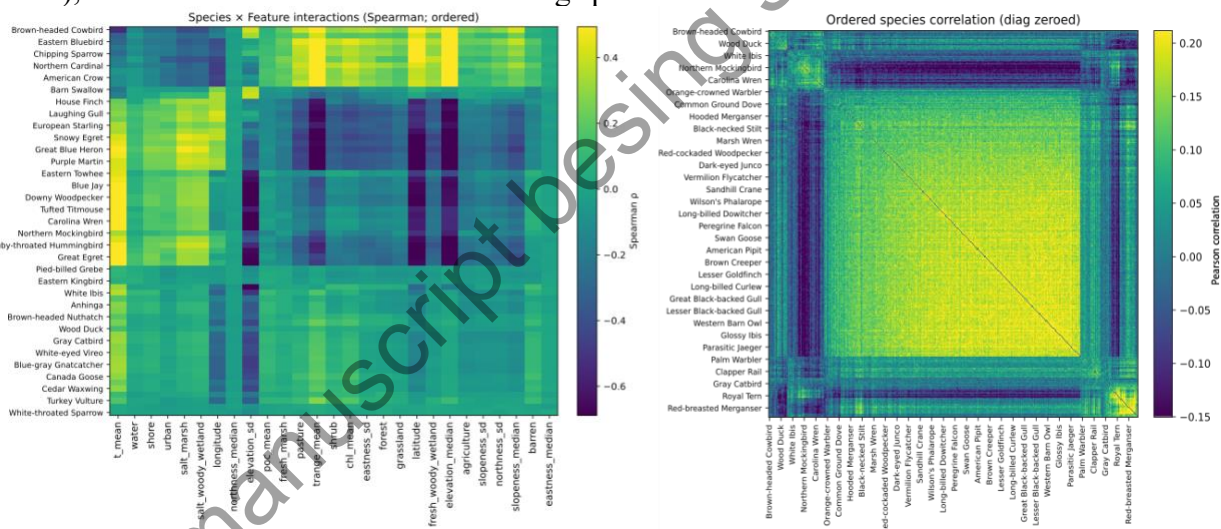

Figure 3. Species-environment correlation (Spearman correlation) and species-species (Pearson correlation) correlation matrices

Because these are (rank-based) species correlations, strong positive links are best read as community clustering around similar environments, while strong negative links point to compositional turnover. Ecologically, when biotic bars rival or exceed the top abiotic bars, local community context becomes a primary predictor—implying that conserving or restoring the assemblage (keystone partners, habitat formers) may be as important as managing the physical environmental envelope.

Together, the deep hurdle model suggests an environment-first niche shape where the species can occur, overlaid by biotic refinement. Species it tends to co-occur with (or avoid) other species once in suitable environments. Where top abiotic and biotic ranks align (e.g., species cluster in the same habitats), expectation is strong co-occurrence "hotspots"; where top biotic ranks

are negative, expect sharp community turnover across short environmental distances. For example, Carolina Wren is positively associated with closed-canopy forest and shrub cover and gentle relief; negatively associated with extensive tidal marsh and open water, indicating avoidance of persistently flooded lowlands. It co-occurs with upland/edge passerines (e.g., woodpeckers, titmice) and segregates from estuarine waders concentrated in marsh cores. The Red-bellied Woodpecker has a strong positive association with mature forests and riparian woods above frequent tidal inundation; a negative correlation with marsh extent and high-salinity estuarine surfaces. Due to habitat preference differences, it exhibits a positive association with the abundance of other forest generalists (e.g., wrens, chickadees) and a negative association with marsh specialists and shoreline waders. Great Egret, however, has a negative population trend with increasing upland passerines that track forested high ground. Therefore, it shows the dominant abiotic drivers separate low-elevation, flooded estuarine habitats (waders) from interior forested or developed higher ground (passerines/commensals). Biotic correlations revealed within-guild co-occurrence (e.g., waders with waders; forest birds with forest birds) and between-guild segregation across sharp marsh–upland transitions.

Functional trait shifts scenarios and scales

Trait probability density (TPD) spaces were plotted in Figure 4 under a historical baseline vs. sea-level-rise (SLR) conditions for two spatial extents: the whole study area (upper row) and the three bay reserves with simulated nutrient/productivity change under SLR (lower row). It was revealed that regional foraging trait space responses to SLR tend to shrink or redistribute occupied trait space, decreasing richness (foraging: $1852.6 \rightarrow 1548.8$) and redundancy (foraging $0.616 \rightarrow 0.328$), increasing evenness (foraging $0.04 \rightarrow 0.10$), and often leading to greater divergence (more extreme strategies) as communities track new habitat configurations. This indicates a contraction of occupied foraging space with a flatter, more uniform distribution inside the remaining space and less functional overlap among species—consistent with SLR removing parts of the coastal niche while equalizing use of the surviving trait combinations.

By contrast, within the three productivity-altered bay reserves, responses are trait-specific: foraging space broadens (more strategies co-existing), movement morpho space compresses toward intermediates, and social behavioral space narrows but differentiates (fewer overlaps, stronger extremes). Specifically, in foraging space, three bay reserves saw richness rise from 1271.3 to 1492.9, evenness rise from 0.03 to 0.09, and redundancy increases from about 0.00 to 1.60. These patterns are consistent with environmental filtering and local productivity effects: regional habitat shifts open new or peripheral trait regions. Regionally, SLR filters out portions of beak morphologies linked to the lowest coastal habitats; in productivity-enhanced reserves, food subsidies mitigate that filter, allowing richer and more overlapping beak strategies to persist.

In the movement trait space, the regional trend is opposite to the foraging space with richness expansion ($3528.2 \rightarrow 5340.7$), higher evenness ($0.12 \rightarrow 0.21$), higher redundancy ($0.02 \rightarrow 1.597$), and greater divergence ($0.61 \rightarrow 0.79$). SLR redistributes communities toward a wider range of wing shapes and more extreme flight strategies, with more species sharing similar flight morphologies across the enlarged space. Understandably, communities diversified toward more varied/edge wing forms to track shifting habitats with SLR, but inside nutrient-altered reserves, habitat confinement favors intermediate flyers and trims the extremes.

In the three bay reserves movement trait space, richness contracts from 7439.9 to 5998.3 while evenness increases from 0.08 to 0.22, redundancy nudges up ($0.513 \rightarrow 0.599$), and

divergence declines from 0.92 to 0.84. Within constrained bay habitats, SLR + productivity produces a more uniformly filled but less extreme movement morphospace—suggesting filtering away from tails toward intermediate flight designs.

Lastly, in the social behavioral space, SLR yields a broader and more evenly used space with slight growth in overlap and more weight toward extremes—consistent with mixed gains at both short- and long-tarsus niches as habitats reorganize (higher richness (79.1 → 113.5), higher redundancy (1.469 → 1.597), and higher divergence increases (0.43 → 0.69)). In reserves, richness decreases modestly (140.4 → 129.0), but evenness (0.08 → 0.21) and divergence (0.60 → 0.88) increase, while redundancy drops (4.006 → 2.529). Productivity shifts, combined with SLR, favor more extreme large species with reduced functional redundancy, even as the absolute trait space shrinks.
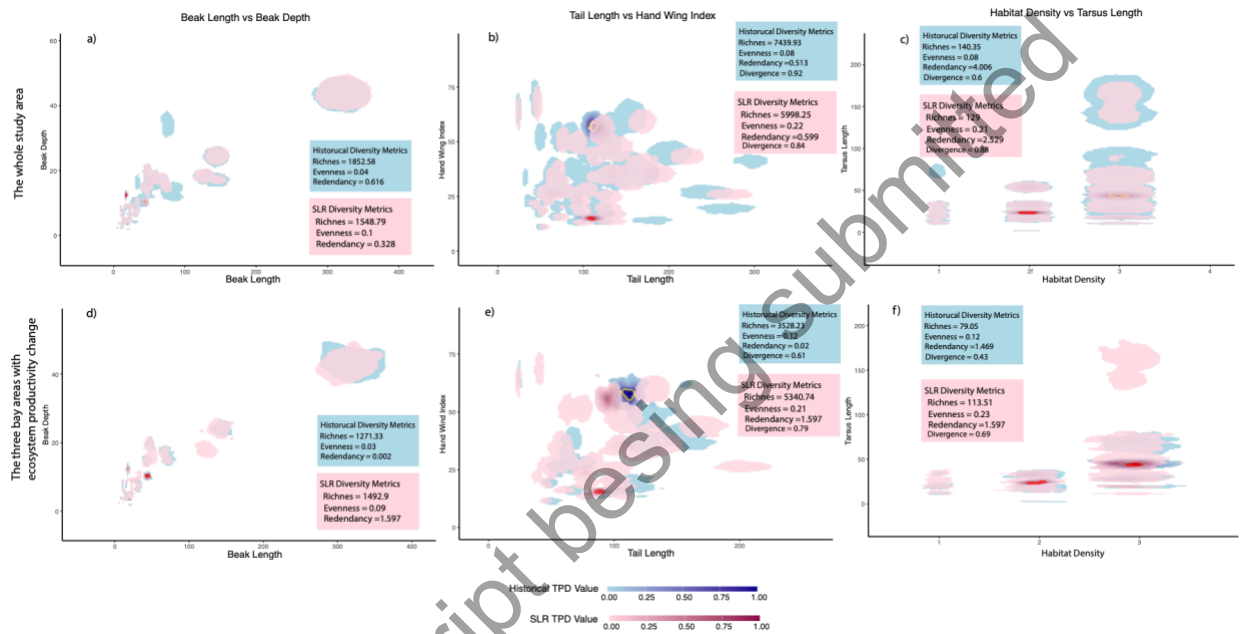

Figure 4. Trait probability density shifts under sea-level rise across regional and reserve scales by three categories of trait space: foraging, movement, and social behavior

Model performance evaluation by habitat preference trait

The confusion matrices were presented for each categorical habitat preference trait in Figure 5. The share of true negatives (top row) and true positives (bottom row) that were predicted as 0 or 1. The bottom-right cell equals recall; the top-right cell is the false-positive rate (FPR). Reported F1, precision (P), and recall (R) summarize each habitat's binary classifier.

The hurdle model is recall-oriented across habitats (R ≈ 0.67–0.84), but precision is low (P ≈ 0.07–0.30), as indicated by the confusion matrices, resulting in a moderate F1 score. This means it usually finds habitat-preferred cases but also raises many false alarms, especially when positives are rare. The general high zero rates across species observations posed challenges to species classification tasks. Best-classified results is produced for Marine birds (F1 = 0.44, P = 0.30, R = 0.84; FPR = 13.8%) and Woodland birds (F1 = 0.43, P = 0.30, R = 0.73; FPR = 15.7%). Many true marine cases are found, though ~14% of non-marine cases are flagged (precision 0.30). For Woodland species, the balanced classification with recall (R 0.73) is strong. The classification for Grassland birds (F1 = 0.12, P = 0.07, R = 0.67; FPR = 8.6%)—recall is decent, but extremely low

precision implies very low prevalence and overlap with other habitat covers. Positive observations are so rare that precision collapses—typical when prevalence is very low.

Urban (Human-modified) bird models exhibit moderate classification performance (F1 = 0.37, P = 0.25, R = 0.71); anthropogenic structures enhance observation quality. Coastal birds prediction results have very high recall (0.80) but low precision (0.15), F1 = 0.25; shoreline cues are broad, so many non-coastal cells get flagged. Riverine is a linear habitat, leading to good sensitivity but many false positives (F1 = 0.26, P = 0.16, R = 0.75). For forest birds, F1 = 0.22 (P = 0.13, R = 0.72). Interior forests are detected, but edges/shared features inflate FPR (13.3%). For future modeling efforts, consider prevalence-aware calibration, additional features (e.g., distance-to-shore, hydroperiod), or hierarchical labeling (e.g., marine/coastal → wetland/riverine → upland subclasses) can potentially increase precision, especially for the habitat trait of grassland, coastal, wetland
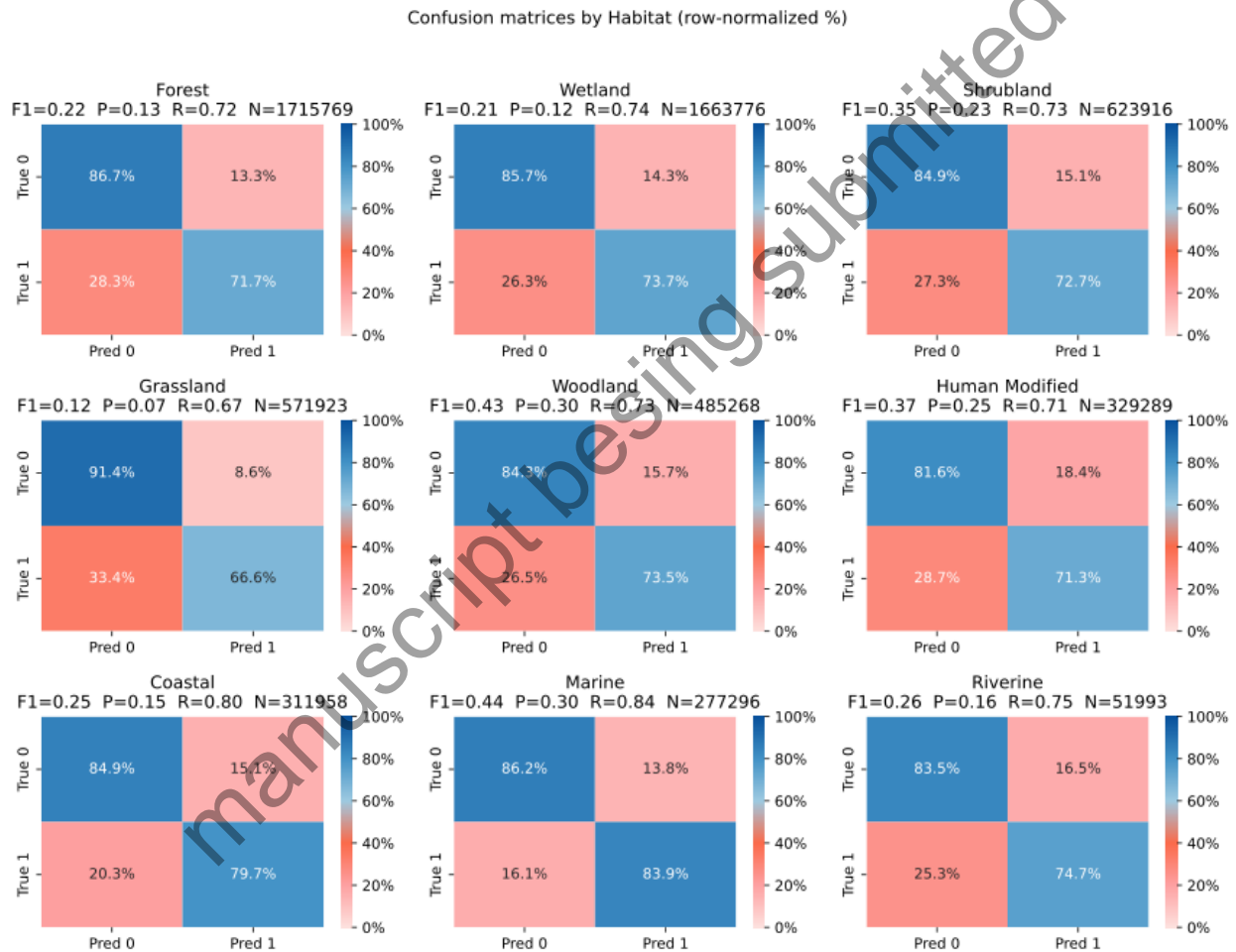

Figure 5. Confusion matrices for occurrence prediction categorized using habitat preference trait (P: precision, R: Recall, N: number of instances)

We also reported the distribution of classification and regression performance by habitat (F1 and RMSE) (Figure 6). F1 summarizes binary accuracy for presence/absence (balance of precision and recall). RMSE reflects regression error for continuous abundance; the normalized RMSE panel rescales errors to be comparable across species that were observed at a large number (outliers).

Again, the signals of Marine and Woodland birds are distinctive (shoreline/open-water; interior canopy), so positives are detected more reliably. Grassland birds and parts of Wetland/Coastal birds have rare positives and overlap with other open habitats, depressing precision, yielding lower F1. Filtering to species with clearer habitat signal shifts F1 upward and tightens spreads in several groups, with the biggest gains where prevalence and edge effects previously hurt precision (e.g., Grassland, Coastal, Wetland). This confirms that within-habitat specialists are classified more consistently than generalists.

Habitats with higher abundance magnitude/variance (e.g., Marine, Wetland/Coastal) show larger raw RMSE simply because errors scale with counts. Conversely, habitats with smaller absolute abundances (e.g., Woodland/Human-modified) tend to show lower raw RMSE. After scaling, relative error remains elevated in transitional, heterogeneous environments (e.g., Coastal, Riverine, Wetland) where fine-scale hydrology and edge effects are hard to capture. Woodland and some Human-modified/Forest areas show lower normalized RMSE, indicating more stable, predictable relationships.
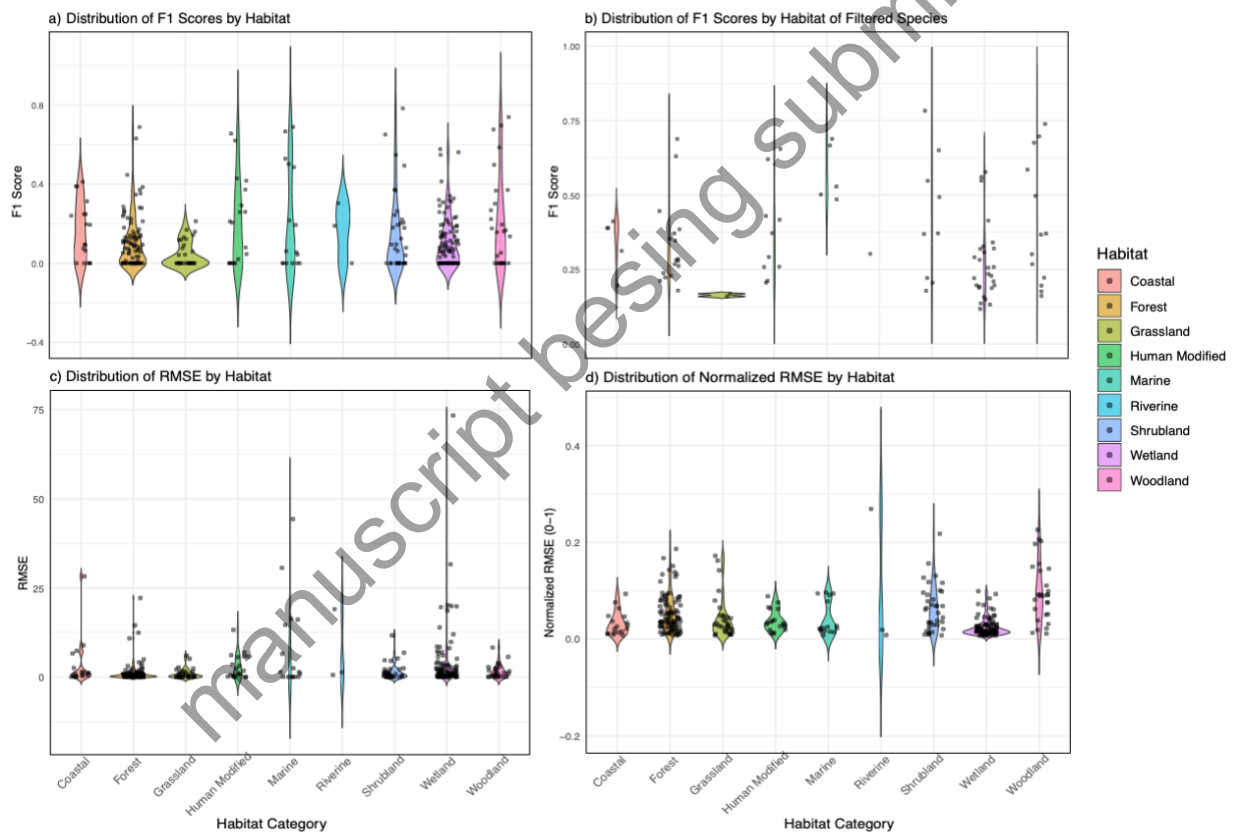

Figure 6. Distribution of classification performance (F1 score) and regression performance (RMSE) by preferred habitats of species

Conclusion

Biodiversity is declining rapidly under global environmental change and intensifying human pressures (Olden et al., 2008). Anticipating these impacts requires ecological forecasts that resolve patterns at both species and community levels to inform conservation and restoration

actions. While species richness and related indices remain informative, this functional diversity study with trait space analysis offered a more mechanistic perspective on ecosystem functioning.

Across the northern Gulf Coast, our results indicate a redistribution rather than uniform collapse of avian abundance in response to sea-level rise (SLR). Wetland specialists (e.g., herons and egrets) lose the lowest coastal hotspots but re-emerge up-estuary and on slightly higher marsh platforms, while forest birds retain interior strongholds and generalists remain broadly persistent with subtle inland shifts. The geography of hotspots, therefore, fragments and pivots toward river mouths and higher micro-topography, consistent with coastal squeeze and landward habitat migration. For conservation and planning, protecting inland migration space for marshes (setback zones, rolling easements), estuarine connectivity (creek networks, sediment supply), and elevated refuge habitats near current shorelines should be prioritized.

Rank-ordered correlations show that a small set of abiotic gradients (e.g., elevation/inundation, wetland extent, shoreline proximity) explains most spatial abundance distribution patterns, with species–species associations acting as biotic refinement: strong within-guild co-occurrence (waders with waders; forest passerines together) and between-guild segregation across sharp marsh–upland transitions. This "environment-first, community-modulated" hierarchy aligns with the mapped inland shifts of wetland birds and the stability of upland assemblages.

Functional trait analyses (TPDs) reveal scale-dependent reorganization. At the regional extent, SLR often expands or redistributes occupied trait space and increases evenness and divergence, indicating a wider spread and greater emphasis on extreme strategies as habitats reorganize. Within reserves where SLR is coupled to simulated nutrient and productivity changes, responses diverge by trait axis: foraging space broadens (more foraging strategies coexist), movement traits compress toward intermediates, and social behavior (size/habitat density) space narrows yet differentiates (reduced redundancy but greater use of extremes). These patterns suggest that local subsidies and confinement can counterbalance or reshape regional filters on function. Therefore, in reserves, it is suggested to pair hydrologic adaptation with productivity and water-quality management to sustain diverse foraging strategies. Because responses are trait- and scale-dependent, monitoring should track guilds and key trait axes, not only species counts.

Model diagnostics by habitat preference show a recall-oriented classifier (generally high sensitivity but low precision), performing best for marine and woodland classes and struggling where positives are rare or overlapping (e.g., grassland, wetland, coastal). This implies that current predictions are well-suited for screening (identifying most true positives) but require threshold tuning, prevalence-aware calibration, and additional habitat cues (e.g., hydroperiod, distance to shore) when high precision is needed for management actions.

Taken together, the evidence supports three conclusions: (i) SLR will shift rather than uniformly reduce bird abundance, concentrating future hotspots in landward-migrating marshes and riverine corridors; (ii) abiotic constraints dominate distributional change, while community structure modulates local composition; and (iii) functional diversity will reorganize, with reserve-scale conditions capable of buffering losses or redirecting trait use. Our results provide a tractable blueprint for conservation actions that secure landward pathways, sustain functional traits, and optimize management at reserve scales—to conserve avian biodiversity in the face of rising sea levels.

References

Assis, J., Fernández Bejarano, S. J., Salazar, V. W., Schepers, L., Gouvêa, L., Fragkopoulou, E., Leclercq, F., Vanhoorne, B., Tyberghein, L., Serrão, E. A., Verbruggen, H., & De Clerck, O. (2024). Bio-ORACLE v3.0. Pushing marine data layers to the CMIP6 Earth System Models of climate change research. *Global Ecology and Biogeography*, *33*(4). https://doi.org/10.1111/geb.13813

Bai, J., Kong, S., & Gomes, C. P. (2021). *Gaussian Mixture Variational Autoencoder with Contrastive Learning for Multi-Label Classification*. http://arxiv.org/abs/2112.00976

Benkendorf, D. J., & Hawkins, C. P. (2020). Effects of sample size and network depth on a deep learning approach to species distribution modeling. *Ecological Informatics*, *60*. https://doi.org/10.1016/j.ecoinf.2020.101137

Bilskie, M. V., Hagen, S. C., Alizad, K., Medeiros, S. C., Passeri, D. L., Needham, H. F., & Cox, A. (2016). Dynamic simulation and numerical analysis of hurricane storm surge under sea level rise with geomorphologic changes along the northern Gulf of Mexico. *Earth's Future*, *4*(5), 177–193. https://doi.org/10.1002/2015EF000347

Botella, C., Joly, A., Bonnet, P., Monestiez, P., & Munoz, F. (2018). A Deep Learning Approach to Species Distribution Modelling. In S. and K. K. and K. A. and B. P. Joly Alexis and Vrochidis (Ed.), *Multimedia Tools and Applications for Environmental & Biodiversity Informatics* (pp. 169–199). Springer International Publishing. https://doi.org/10.1007/978-3-319-76445-0_10

Chen, Y., Gu, Z., & Zhan, X. (2024). stemflow: A Python Package for Adaptive Spatio-Temporal Exploratory Model. *Journal of Open Source Software*, *9*(94), 6158. https://doi.org/10.21105/joss.06158

Christin, S., Hervet, É., & Lecomte, N. (2019). Applications for deep learning in ecology. In *Methods in Ecology and Evolution* (Vol. 10, Issue 10, pp. 1632–1644). British Ecological Society. https://doi.org/10.1111/2041-210X.13256

Davis, C. L., Bai, Y., Chen, D., Robinson, O., Ruiz-Gutierrez, V., Gomes, C. P., & Fink, D. (2023). Deep learning with citizen science data enables estimation of species diversity and composition at continental extents. *Ecology*, *104*(12). https://doi.org/10.1002/ecy.4175

de Rivera, O. R., Blangiardo, M., López-Quílez, A., & Martín-Sanz, I. (2019). Species distribution modelling through Bayesian hierarchical approach. *Theoretical Ecology*, *12*(1), 49–59. https://doi.org/10.1007/s12080-018-0387-y

Fick, S. E., & Jijmans, R. J. (2017). WorldClim 2: new 1km spatial resolution climate surfaces for global land areas. *International Journal of Climatology*, *37*(12), 4302–4315.

Fink, D., Hochachka, W. M., Zuckerberg, B., Winkler, D. W., Shaby, B., Munson, M. A., Hooker, G., Riedewald, M., Sheldon, D., & Kelling, S. (2010). Spatiotemporal exploratory models for broad-scale survey data. *Ecological Applications*, *20*(8), 2131–2147. https://doi.org/10.1890/09-1340.1

Hirn, J., Sanz, V., García, J. E., Goberna, M., Montesinos-Navarro, A., Navarro-Cano, J. A., Sánchez-Martín, R., Valiente-Banuet, A., & Verdú, M. (2024). Transfer learning of species co-occurrence patterns between plant communities. *Ecological Informatics*, *83*. https://doi.org/10.1016/j.ecoinf.2024.102826

Johnston, A., Auer, T., Fink, D., Strimas-Mackey, M., Iliff, M., Rosenberg, K. V., Brown, S., Lanctot, R., Rodewald, A. D., & Kelling, S. (2020). Comparing abundance distributions and range maps in spatial conservation planning for migratory species. *Ecological Applications*, *30*(3). https://doi.org/10.1002/eap.2058

Lek, S., Belaud, A., Baran Ioannis Dimopoulos, P., Delacoste, M., Belaud, A., Baran, P., Delacoste, M., & Lek, S. (1996). Role of some environmental variables in trout abundance models using neural networks. *Aquatic Living Resources*, *9*, 23–29.

Nielsen, M. (2015). *Neural Networks and Deep Learning*. http://neuralnetworksanddeeplearning.com

Olden, J. D., Lawler, J. J., & Poff, N. L. (2008). Machine learning methods without tears: A primer for ecologists. In *Quarterly Review of Biology* (Vol. 83, Issue 2, pp. 171–193). https://doi.org/10.1086/587826

O'Neill, B. C., Tebaldi, C., Van Vuuren, D. P., Eyring, V., Friedlingstein, P., Hurtt, G., Knutti, R., Kriegler, E., Lamarque, J. F., Lowe, J., Meehl, G. A., Moss, R., Riahi, K., & Sanderson, B. M. (2016). The Scenario Model Intercomparison Project (ScenarioMIP) for CMIP6. *Geoscientific Model Development*, *9*(9), 3461–3482. https://doi.org/10.5194/gmd-9-3461-2016

Phillips, S. (2008). A Brief Tutorial on Maxent. AT&T Research. *AT&T Research*, 1–38.

Rammer, W., & Seidl, R. (2019). Harnessing Deep Learning in Ecology: An Example Predicting Bark Beetle Outbreaks. *Frontiers in Plant Science*, *10*. https://doi.org/10.3389/fpls.2019.01327

Sullivan, B. L., Wood, C. L., Iliff, M. J., Bonney, R. E., Fink, D., & Kelling, S. (2009). eBird: A citizen-based bird observation network in the biological sciences. *Biological Conservation*, *142*(10), 2282–2292. https://doi.org/10.1016/J.BIOCON.2009.05.006

Vinuesa, R., & Sirmacek, B. (2021). *Interpretable deep-learning models to help achieve the Sustainable Development Goals*. http://arxiv.org/abs/2108.10744